JACS
JOURNAL OF THE AMERICAN CHEMICAL SOCIETY
Article
pubs.acs.org/JACS

Chemically Optimizing Operational Efficiency of Molecular Rotary Motors

Jamie Conyard,[†] Arjen Cnossen,[‡] Wesley R. Browne,[‡] Ben L. Feringa,[‡] and Stephen R. Meech*[,†]

[†]School of Chemistry, University of East Anglia, Norwich Research Park, Norwich NR4 7TJ, United Kingdom
[‡]Stratingh Institute for Chemistry, University of Groningen, Nijenborgh 4, 9747AG Groningen, The Netherlands

Supporting Information

ABSTRACT: Unidirectional molecular rotary motors that harness photoinduced cis−trans (E−Z) isomerization are promising tools for the conversion of light energy to mechanical motion in nanoscale molecular machines. Considerable progress has been made in optimizing the frequency of ground-state rotation, but less attention has been focused on excited-state processes. Here the excited-state dynamics of a molecular motor with electron donor and acceptor substituents located to modify the excited-state reaction coordinate, without altering its stereochemistry, are studied. The substituents are shown to modify the photochemical yield of the isomerization without altering the motor frequency. By combining 50 fs resolution time-resolved fluorescence with ultrafast transient absorption spectroscopy the underlying excited-state dynamics are characterized. The Franck−Condon excited state relaxes in a few hundred femtoseconds to populate a lower energy dark state by a pathway that utilizes a volume conserving structural change. This is assigned to pyramidalization at a carbon atom of the isomerizing bridging double bond. The structure and energy of the dark state thus reached are a function of the substituent, with electron-withdrawing groups yielding a lower energy longer lived dark state. The dark state is coupled to the Franck−Condon state and decays on a picosecond time scale via a coordinate that is sensitive to solvent friction, such as rotation about the bridging bond. Neither subpicosecond nor picosecond dynamics are sensitive to solvent polarity, suggesting that intramolecular charge transfer and solvation are not key driving forces for the rate of the reaction. Instead steric factors and medium friction determine the reaction pathway, with the sterically remote substitution primarily influencing the energetics. Thus, these data indicate a chemical method of optimizing the efficiency of operation of these molecular motors without modifying their overall rotational frequency.

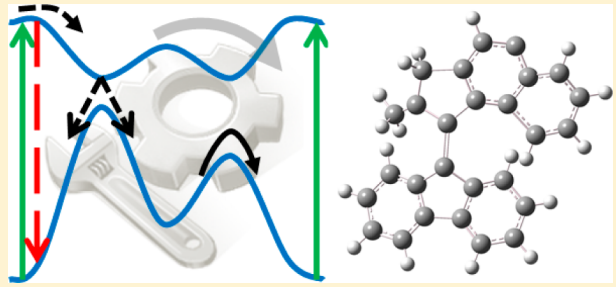

INTRODUCTION

Biological motors are capable of driving processes as diverse as locomotion and intracellular transport.[1,2] Such motors operate with high efficiency, often by converting chemical energy into molecular motion.[3] These observations of the fine control of motion in living systems have stimulated great interest in mimicking such behavior in synthetic molecular nanomachines. The elegant complexity of the multiprotein complexes that make up biological motors is currently beyond the reach of synthetic chemistry,[4] stimulating the search for simpler more robust alternatives.

A promising design for a synthetic rotary motor based on chiral overcrowded alkenes was introduced by Feringa and co-workers.[5−7] These compounds (e.g., 1a-R, Figure 1) overcome two important challenges in the design of molecular motors.

First, the energy required for the power stroke is obtained through absorption of light, with the motors utilizing excited-state cis−trans (or E−Z) isomerization to convert incident light energy into mechanical motion. Second the configuration at the stereogenic center imposes unidirectional motion, a key component in a rotary motor that distinguishes these compounds from simple molecular photoswitches. The mode of operation is illustrated in Figure 1.[8] The motors comprise a lower "stator" fluorene ring linked to an upper "rotor" by the ethylenic "axle". Electronic excitation localized on the ethylenic bond leads to a photoisomerization in which the rotor rotates relative to the stator about the axle to yield the isomer 1b-R. As a consequence of the steric interaction between the aromatic groups of the rotor and stator in 1a-R this motion occurs overwhelmingly in one direction. In 1a-R the methyl group at the stereogenic center adopts an axial conformation, while in 1b-R it is equatorial. A thermally activated helix inversion occurs on the ground-state surface, which returns the methyl group to the more energetically favorable axial orientation (1c-R). This reintroduces the steric barrier to rotation in the reverse direction. Thus, this helix inversion acts as a "lock" which on absorption of a second photon forces the photoisomerization to occur selectively in the original direction to yield 1d-R. This is then followed by a second thermal helix inversion to complete one complete rotation. Under constant irradiation, the cycle is repeated resulting in repetitive unidirectional rotation of the rotor relative to the stator.

Received: April 25, 2014
Published: June 11, 2014

   dx.doi.org/10.1021/ja5041368 | J. Am. Chem. Soc. 2014, 136, 9692−9700

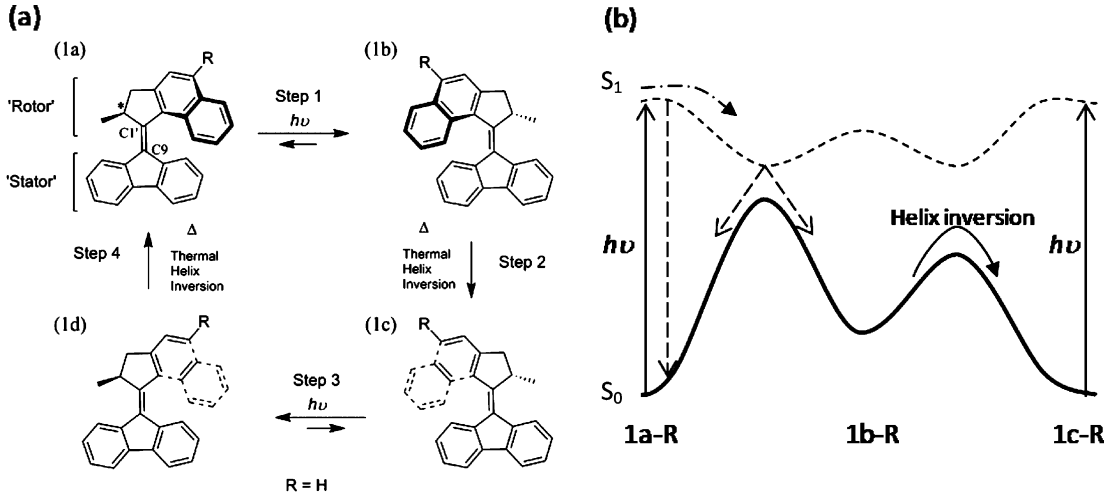

Figure 1. (a) The photocycle of unidirectional rotation in a molecular motor. The stable ground state 1a-R absorbs a photon which stimulates a cis−trans (E−Z) isomerization to populate 1b-R. This metastable state undergoes a thermal helix inversion in the ground state to form 1c-R. Consequently absorption of a second photon leads to cis−trans isomerization in the original direction to form 1d-R, and a second thermal helix inversion generates 1a-R giving one full rotation. The position of R and the substituents (R = CN, Cl, H, OMe) were chosen to modify electron-donor strength without altering the steric interactions between the rings. (b) Schematic potential energy surfaces indicating the states probed in the current study (dashed lines).

The rate-determining step in this process is the thermal helix inversion, which consequently limits the rotation speed of the motor. Considerable synthetic effort has been focused on reducing the barrier to helix inversion, and rotation rates in the MHz regime have been achieved.[9,10] Less attention has been paid to the photochemical step, although it is the efficiency of cis−trans isomerization that determines the overall photochemical conversion efficiency of the motor. Recently we reported the ultrafast dynamics of the parent compound 1a-H.[11] Ultrafast fluorescence spectroscopy revealed that the primary photochemical step, a relaxation from the initial Franck−Condon excited state, occurred within 100 fs, populating an energetically lower dark (i.e., nonfluorescent) region of the excited-state surface (labeled "dark state" hereafter). Transient absorption showed that this state subsequently decayed on a picosecond time scale to the ground state. This ultrafast primary process was accompanied by coherent oscillations associated with vibrational coherences in the excited electronic state. These data suggested two ways in which to modify the photochemical efficiency of the molecular motor. First, one can imagine excitation schemes exploiting coherent control, utilizing the observed vibrational coherences. This possibility has indeed been considered theoretically.[12,13] However, experimentally this presents many challenges, especially as the coherences were observed to decay on a subpicosecond time scale.[11] In this paper we consider the alternative approach of chemically modifying 1a-H with substituents designed to influence the isomerization reaction without altering the stereochemistry (Figure 1).[14,15]

The substituents (for systematic names see Supporting Information) considered are the electron-withdrawing cyano and chloro (R = CN, Cl) and the electron-donating methoxy (R = OMe) groups, which are located at the 5′ position and are thus in direct conjugation with the central double bond, which is mainly involved in the HOMO−LUMO transition that dominates the S_0−S_1 excitation. It was anticipated that an electron donor would increase the single bond character and thus enhance the rate of thermal helix inversion. Interestingly it was found that these substituents had a negligible effect on the barrier in the ground-state potential energy surface.[16] Instead it was found that the photostationary state achieved under continuous irradiation was strongly dependent on both the substituent and the solvent.[10] This suggests that the principal effect of the substituent is on the excited-state reaction. Here, we probe the steady-state quantum yield, ultrafast fluorescence and transient absorption of 1a-R. The sub 100 fs to tens of picosecond dynamics are interpreted in terms of a substituent dependence of the shape of the excited-state potential energy surface. These data therefore suggest a route to rationally designing motors of high efficiency in a manner that is independent of the thermal isomerization step which controls the rotational frequency.

RESULTS AND DISCUSSION

Ground-State Structure and Steady-State Quantum Yield. The steady-state absorption and emission spectra for 1a-R are shown in Figure 2. All substituents give rise to a red shift in the absorption compared to 1a-H. Spectral shifts were investigated by TD-DFT calculations (see Supporting Information). For R = CN, Cl the LUMO is stabilized more than the HOMO, while for R = OMe the HOMO is destabilized more than the LUMO, such that in both cases a red shift results. The emission is weak, with the fluorescence quantum yield estimated to be $<10^{-4}$ in all cases. The electronic spectra were found to be only weakly sensitive to solvent (absorption and emission maxima are presented in the Table S1). In-line with this, the Stokes shift was also only a weak function of solvent polarity, although it is consistently slightly larger in nonpolar than in polar solvents (Table S1). The latter result shows that there is no significant change in dipole moment between the ground and fluorescent excited states, which in-turn suggests that there is no major change in the degree of intramolecular charge transfer between these two states.

The effect of substituents on the efficiency of the motor was assessed through measurements of the photochemical quantum yield of the isomerization from 1a-R to 1b-R (Figure 1). The quantum yields were measured under steady-state conditions compared to decomposition of ferrioxalate as a standard (see Supporting Information) and are presented in Table 1. Significantly the yield for the reverse photoisomerizarion was

dx.doi.org/10.1021/ja5041368 | J. Am. Chem. Soc. 2014, 136, 9692−9700

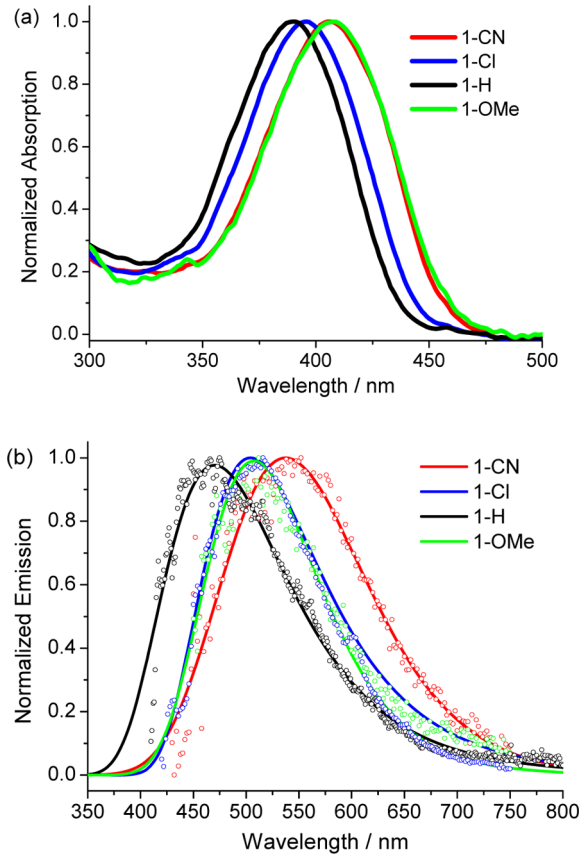

Figure 2. (a) Absorption spectra of 1a-R in DCM. (b) Emission spectra in DCM excited at 370 nm (data points are shown fit to a log-normal function). A solvent Raman contribution has been subtracted, mainly affecting the blue edge of the emission. All spectra are peak normalized.

Table 1. Quantum Yield for the 1a-R to 1b-R Reaction[a]

substituent	quantum yield
1a-CN	0.2
1a-Cl	0.15
1a-H	0.14
1a-OMe	0.048

[a]365 nm irradiation, accuracy ±5%.

larger (Supporting Information), which limits the efficiency of the motors (although they remain unidirectional). In Table 1 it is evident that the previously reported negligible effect of substituent on the rate of the ground-state inversion (e.g., 1b-R to 1c-R) is not reflected in the efficiency of photochemical isomerization.

The quantum yield for isomerization varies by a factor of 4 across the series, in the order OMe < H ≈ Cl < CN, i.e., electron-withdrawing groups conjugated to the ethylenic "axle" enhance the quantum yield of isomerization. The ground-state structure was investigated further by DFT calculations. Although the data (see Table S2) are consistent with the expectation that electron donor substituents weaken the "axle" double bond, the effects are minor. For R = OMe a <0.2 pm lengthening of the bond was calculated, accompanied by a 0.3° increase in twist angle and 0.2° decrease in pyramidalization at C1. For the acceptor R = CN the shifts are in the opposite direction, as expected, but the effect was again minor (Table S2). Such small differences in structure are consistent with the previously reported negligible effect on the rate of thermal

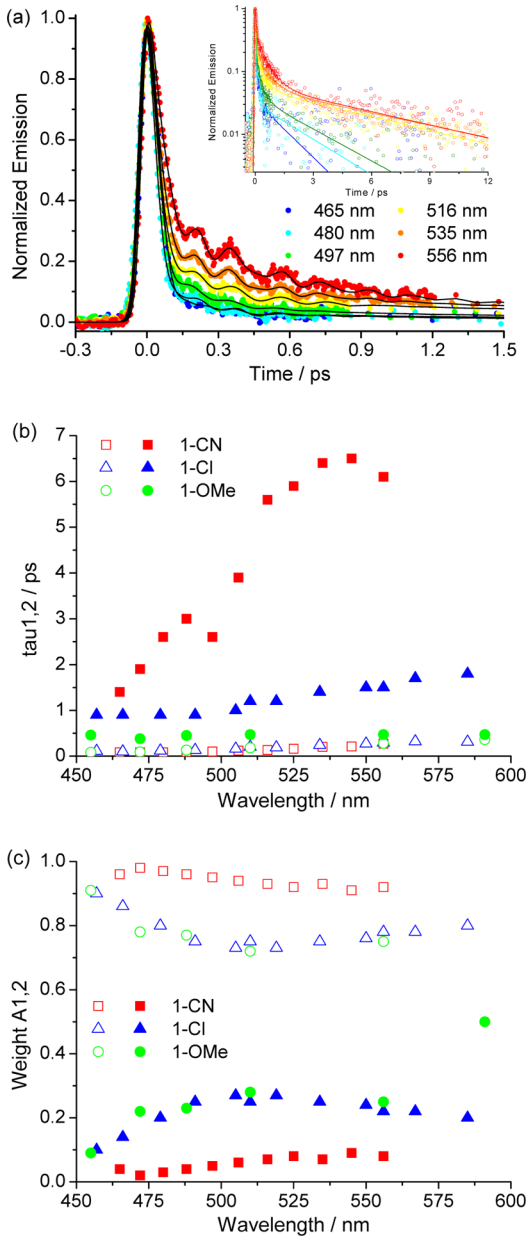

Figure 3. (a) Fluorescence up-conversion data for 1a-CN in DCM measured as a function of the emission wavelength after excitation at 400 nm. The fitted lines are convolutions of (1) with the instrumental response function (obtained by up-conversion of Raman scattered light). The inset shows the same data on a log intensity scale. (b) A plot of the fluorescence decay times extracted from the fit of the data to (1), see also Table S3. R = −CN (red), −Cl (blue), and −OMe (green); open symbols are for τ_1, filled for τ_2. Where two components were needed to fit the fastest decay in 1a-CN (see text) the weighted average is taken. (c) The corresponding weights of each decay component. For fitting data associated with the damped oscillators see Supporting Information.

inversion in the ground state. Thus, the significant effect of the substituent on the quantum yield (Table 1) but on neither the rate continuous for inversion nor the ground-state structure suggests that the principal substituent effect is on excited-state processes.

Ultrafast Fluorescence. Figure 3 shows the fluorescence decay data for 1a-CN in dichloromethane (DCM) measured with 50 fs time resolution (data for the other 1a-R compounds are presented in the Figure S1). These data share many

dx.doi.org/10.1021/ja5041368 | J. Am. Chem. Soc. 2014, 136, 9692−9700

common features with our previous report on the fluorescence of 1a-H[11] but reveal several important differences. For all substituents the decay is ultrafast, consistent with the low fluorescence quantum yield, and shows non-single exponential decay kinetics. Further, the decay is a strong function of emission wavelength, increasing in mean relaxation time as the wavelength observed is tuned to the red side of the spectrum (Figure 3). The fluorescence decay is accompanied by strong oscillatory features, which arise from coherent vibrational dynamics in the electronically excited state. The observation of such coherent dynamics in time-resolved fluorescence allows an unambiguous assignment to excited-state modes, since the ground state cannot contribute; additional data are required to make such an assignment from pump–probe spectroscopy.

To account for these features all data were fitted to sums of exponentially decaying components and damped oscillator functions:

$$F(t) = \sum_{i=1}^{n} A_i \exp(-t/\tau_i) + \sum_{j=1}^{m} A_j \sin(\omega_j t + \varphi_j)\exp(-t/\tau_{Dj}) \quad (1)$$

where τ_i is a fluorescence decay times of amplitude A_i and τ_{Dj} is the damping time associated with an oscillators of frequency ω_j, phase ϕ_j, and amplitude A_j. The minimum n and m sufficient to recover random residual plots were used, which for 1a-CN required $n = m = 3$, while for the other three derivatives $n = 2$ and $m = 3$ was sufficient. The non-single exponential ($n > 1$) character of the fluorescence decay arises when population dynamics on a potential energy surface are probed by emission at a single wavelength. Thus, the relatively more complex decay for 1a-CN may simply reflect its different PES. The fluorescence decay data as a function of wavelength are plotted in Figure 3b,c and the complete numerical data are included in Table S3.

There is a clear trend in the wavelength-dependent decay as a function of the electronic character of the substituent (Figure 3b,c). The amplitude of the ultrafast (hundreds of femtoseconds) decay component is largest for the most electron-withdrawing 1a-CN group, while the slower (>1 ps) decay time is of low weight. In contrast, for 1a-OMe both fast and slow components are of similar decay time, and there is a convergence in both decay times and amplitudes as the observation wavelength is moved to the red. For the weakly electron-withdrawing substituent, R = Cl, the data are intermediate between these two extremes and close to the values reported previously for 1a-H (Supporting Information).

There are also distinct differences in the pattern of the oscillations. For R = CN, Cl, and H a low-frequency critically damped mode of 3–4 THz (ca. 100 cm^{-1}) was required to fit the data. This mode is absent from fits to the OMe data (Table S3). This absence is illustrated in the frequency domain representation of the isolated oscillatory response (Figure 4). Previously we proposed that the low frequency of this mode and the correspondence between its damping time, τ_{D1}, and the fastest population relaxation time, τ_1, was consistent with its involvements in the reaction coordinate.[11] On the basis of the solvent viscosity dependence and through a comparison with existing quantum dynamics calculations it was proposed that this mode could be assigned to pyramidalization at C9.[17,18] Thus, the absence of this mode in the electron-donating 1a-OMe is significant. We return to this point below. Two higher frequency underdamped modes are found for R = CN, Cl, and H and three for OMe (Figure 4, Table S3). The relatively long damping times suggest these can be assigned as "spectrator modes" not involved in the reaction coordinate.[19]

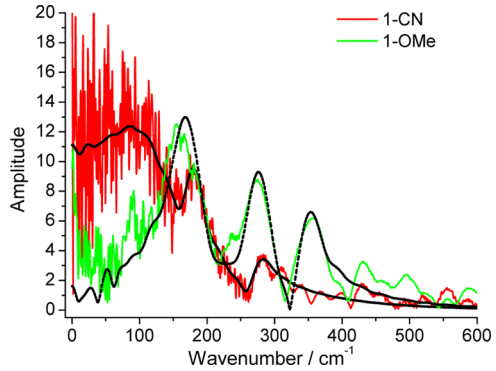

Figure 4. A frequency domain representation of the coherent vibrational dynamics. The data were obtained by subtracting the exponential relaxation terms from the fluorescence decays (at 516 and 510 nm for 1a-CN and 1a-OMe, respectively) and taking the Fourier transform of the residual. The black lines are the Fourier transform of the oscillatory part of eq 1 fit to the same data, showing good agreement between the two.

To extract the molecular dynamics on the excited-state potential energy surface a three-dimensional intensity–wavelength–time surface was created by area normalizing each wavelength-resolved fluorescence decay to the corresponding intensity in the steady-state emission spectrum. The resulting three-dimensional surface and selected intensity–time slices are shown for 1a-Cl in Figure 5, with the results for other 1a-R presented in Supporting Information (Figure S2).

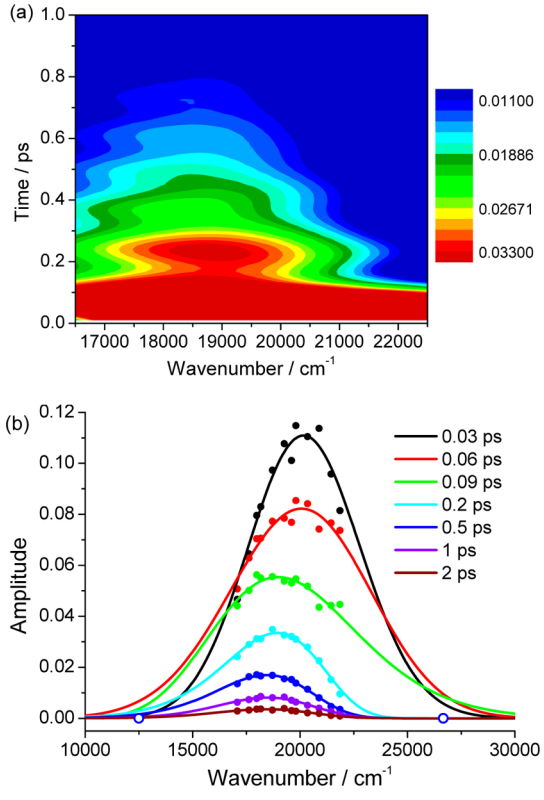

Figure 5. Time resolved spectra measured for 1a-Cl. (a) The three-dimensional intensity–energy–time surface and (b) spectra (intensity–energy slices) as a function of time. The data in (b) (points) were fit to a log-normal function (solid line). As the spectra are very broad the fit was constrained on the low- and high-energy sides as described elsewhere.[11]

dx.doi.org/10.1021/ja5041368 | J. Am. Chem. Soc. 2014, 136, 9692–9700

The time-resolved spectra are shown fit to a log-normal function (Figures 5 and S2), and these fits are analyzed for their time-dependent width, first moment, and integrated intensity, with the results presented in Figure 6. The mean frequency shifts to the red by about 2000 cm^{-1} in <500 fs for both 1a-CN and 1a-OMe. The spectra appear to blue shift at later times, but the amplitude is very low (Figure 5) and the uncertainty large. For both solutes the mean frequency exhibits oscillations that correspond to the higher frequency underdamped modes. These oscillations arise when broadband coherent excitation of vibronic transitions launches a wavepacket on the excited-state surface which has the effect of modulating the energy spacing between the ground and excited states at the frequency of the vibrations.[20−23] This gives rise to the oscillations observed in the mean frequency of the emission (Figure 6).

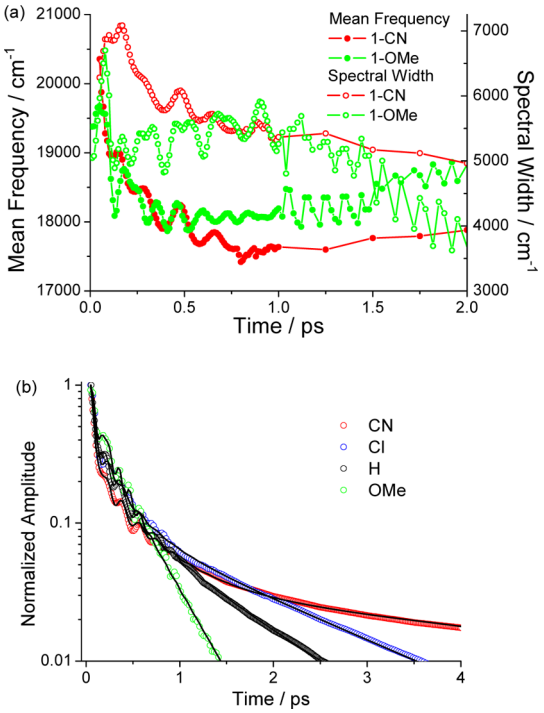

Figure 6. Log-normal parameters extracted from fits to the time-dependent fluorescence of 1a-R. (a) Mean frequency and spectral width for 1a-CN and 1a-OMe. (b) Time-dependent integrated area (reflecting excited-state population dynamics) of the log-normal fits to all 1a-R.

In 1a-R these oscillations are superimposed on an overall red shift (energy relaxation) which we associate with motion along the reaction coordinate, as discussed further below. During the red shift the spectrum also initially broadens to reach a constant value (Figure 6). The population dynamics are best represented by the integrated area of the time-resolved spectra shown in Figure 6b. Significantly oscillatory dynamics are also evident in the integrated spectra, which shows that the coherently excited vibrations are coupled to the transition moment as well as to the transition frequency.[24] The integrated data were fit to (eq 1) above, and the results are shown in Table 2 for the population decay and Table S4 for the oscillatory part.

For R = CN, Cl, H the data required three exponential decay terms and three frequencies, while for 1a-OMe only two exponential decay terms were required. In all four cases the population decay can be broadly represented by a 100−200 fs decay and a longer component, so for the purposes of comparison the two fastest exponential terms in R = CN, Cl, H were averaged as $\langle\tau_1\rangle$, while for OMe $\langle\tau_1\rangle = \tau_1$. Overall, the electron-withdrawing substituent (1a-CN) gives rise to a more dominant ($A_1 + A_2$) and faster fast, $\langle\tau_1\rangle$, population decay component than for 1a-H but a slower long decay (τ_3), whereas the opposite is true for the electron-donating substituent (1a-OMe). In addition, the longer slow decays associated with electron-withdrawing groups are of low amplitude (Table 2, Figure 6b). In all cases the fit to (eq 1) recovers the same frequencies as were extracted from the single wavelength analyses (Table S4), and the low frequency 3−4 THz response was again absent from the OMe data.

Table 2. Population Dynamics for 1a-R Obtained from the Time-Dependent Integrated Area of Time-Resolved Fluorescence (Figure 6b)[a]

substituent	τ_1/ps	A_1	τ_2/ps	A_2	$\langle\tau_1\rangle$/ps	τ_3/ps	A_3
1-CN	0.07	0.77	0.44	0.19	0.14	4.46	0.04
1-Cl	0.10	0.67	0.33	0.24	0.16	1.55	0.09
1-H	0.08	0.77	0.32	0.16	0.12	1.02	0.07
1-OMe	0.11	0.54	–	–	0.11	0.37	0.46

[a]The data were fit to eq 1 and $\langle\tau_1\rangle$ is the weighted average of the two components required to fit the fast relaxation.

Transient Absorption. Ultrafast fluorescence spectroscopy yields the most direct information on the primary processes in excited-state dynamics. However, it necessarily misses the subsequent evolution in the dark excited-state and on the ground-state surface. For such data additional experiments are required. The transient absorption difference spectra for 1a-CN and 1a-OMe are shown in Figure 7 (and for the other substituents in Figure S3). Three features are apparent. First, a red-shifted transient absorption relaxing on the picosecond time scale is observed. This new state appears within the 300 fs time resolution of the experiment and is assigned to excited-state absorption. These spectra reveal the trend that as the electron-withdrawing character of the substituent increases the excited-state absorption shifts further to the red.

Second, a weak long-lived (>100 ps) transient absorption is observed at 450−500 nm, which is assigned to the photochemically generated unstable form of the ground state, 1b-R (or its precursor; a more definite assignment would require measurements on the nanosecond time scale). Third, a bleach (negative ΔOD) is observed below 450 nm and is assigned to the ground state (by comparison with the absorption spectrum, Figure 2); this bleach also recovers on the picosecond time scale. Finally, by shifting the observation window to focus on the 550−700 nm region, a second bleach signal was observed on the low-energy edge of the transient absorption (Figure S4). Since there is no ground-state absorption in 1a-R beyond 500 nm we assign this feature to residual stimulated emission, consistent with the very broad fluorescence spectra (Figure 2).

The data for all 1a-R have been fit to sums of exponentials at the peak wavelength of the ground-state bleach and the transient absorption. No rise time or other spectral evolution was observed corresponding to the dominant 100 fs fluorescence decay time, consistent with the 300 fs time resolution of the transient absorption experiment. However, we can immediately conclude that the 100 fs fluorescence decay does not correspond to fast internal conversion back to the ground state, from both the persistence of ground-state bleach on that time scale and the sub 300 fs formation of a picosecond lifetime transient absorption (Figure 7). Evidently the ultrafast fluorescence

dx.doi.org/10.1021/ja5041368 | J. Am. Chem. Soc. 2014, 136, 9692−9700

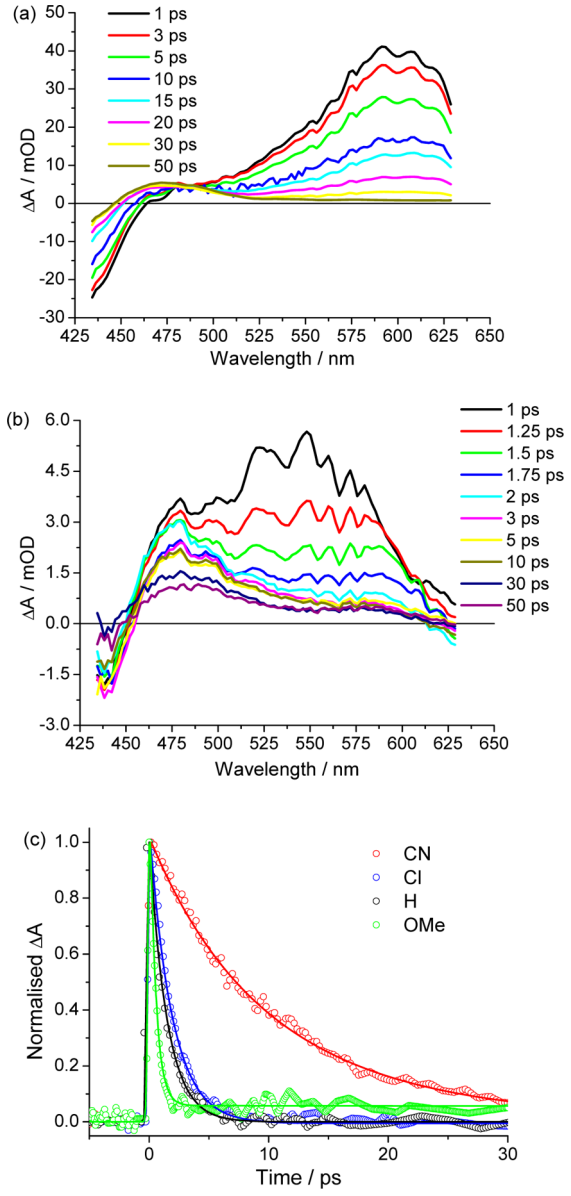

Figure 7. Transient absorption spectra for (a) 1a-CN and (b) 1a-OMe. (c) The decay of the transient absorption for all 1a-R measured at the wavelength of maximum ΔA in each case.

reports fast population relaxation on the excited-state surface out of the Franck–Condon excited state. In all cases the red-shifted excited-state absorption is much longer lived than the fastest component observed in the fluorescence, so it is assigned to a relaxed dark excited state, rather than the Franck–Condon state.

The transient absorption kinetics are shown in Figure 7c, where it is immediately noticeable that 1a-CN has by far the slowest decay. It is also apparent that as the electron-donating character of the substituent increases the transient decay rate increases, such that, for 1a-OMe, the decay is at the limit of our time resolution and similar to the fluorescence decay rate. The fit parameters are shown in Table 3 for both transient decay and bleach recovery. For 1a-CN the transient data sets were best fit by a biexponential function with 5 ± 1 ps and 13 ± 2 ps components, but for comparison the weighted average is reported in Table 3. It is apparent from these data that the picosecond decay of the transient absorption matches the ground-state recovery time, showing that there is a direct relaxation from the relaxed excited state back to the ground state. Significantly there is also a strong correlation between the slowest component in the fluorescence decay and the decay time of the transient absorption (Table 3).

Table 3. 1a-R Transient Absorption Kinetics in DCM[a]

substituent	dark-state lifetime/ps	ground-state recovery/ps	τ_3 fluorescence/ps
1-CN	10.41	11.86	4.46
1-Cl	1.86	1.83	1.55
1-H	1.47	–	1.02
1-OMe	0.51	0.53	0.37

[a]The data were fit to a single or (for 1a-CN) a sum of two exponentials terms. In the latter case the weighted average is reported. Measurements were made for both the transient decay and ground-state recovery, and both are compared with the slowest component measured from time resolved fluorescence, τ_3.

This suggests that the dark state is coupled to the Franck–Condon emissive state. The exception is for 1a-CN where the transient absorption decays even more slowly than the longest fluorescence decay time. It is possible that this is an artifact reflecting the very low weight for the long-lived component of 1a-CN in the time-resolved fluorescence (Figure 3) and its multiexponential decay character, which tends to bias the 100 fs resolution fluorescence observations to earlier decay times. However, we cannot explicitly rule out the possibility that another longer lived intermediate appears in the 1a-CN photocycle, which subsequently decays to the ground state; there is however no spectroscopic evidence for this state. To further probe this assignment the stimulated emission gain was measured as a function of time (Figure S4b). Although the data are too noisy for reliable analysis they clearly decay on an identical time scale to the transient absorption (Figure S4b), consistent with an assignment in which the long-lived emission is fed by coupling to the long-lived "dark" state, analogous to thermally activated delayed fluorescence.

Thus, a consistent picture emerges for the excited-state dynamics of 1a-R. The time-resolved fluorescence reports an ultrafast (Figure 3) energetically downhill (Figure 5) relaxation from the Franck–Condon excited state on a 100 fs time scale. This relaxation populates a "dark" state on the excited-state surface. This dark state relaxes on a picosecond time scale to the ground-state surface from which it may either populate the 1b-R form or relax back to its initial ground state (Figure 7). The intermediate "dark" state establishes a thermal equilibrium with the emissive state, to which it thus contributes the observed slow fluorescence decay time (Table 3). The dark state is longer lived in the case of electron-withdrawing substituents, but in that case it contributes a smaller weight to the fluorescence decay.

Self-Consistent Model for Substituent Effects. In Figure 8 a two-dimensional representation of a multidimensional reactive potential energy surface is presented, which captures the essence of the substituent-dependent dynamics of molecular rotary motors reported above. Optical excitation populates the emissive (bright) Franck–Condon excited state. This state is unstable to structural reorganization, such that an energetically downhill relaxation occurs in about 100 fs to populate a "dark" excited state (Figure 8a). This relaxation is not simply exponential but involves both excitation of coherent oscillations along a critically damped 3–4 THz (ca 100 cm^{-1}) mode and a shift to lower energy yielding a rapid red shift and

dx.doi.org/10.1021/ja5041368 | J. Am. Chem. Soc. 2014, 136, 9692–9700

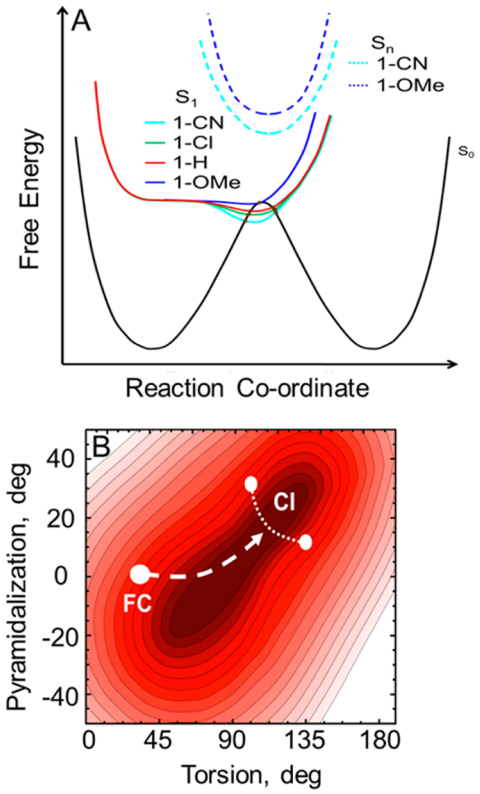

Figure 8. (a) Potential energy surfaces for the primary excited-state dynamics of 1a-R showing the proposed increase in depth of potential well for electron-withdrawing R. (b) Schematic two-dimensional representation of the torsional and pyramidalization coordinates assigned to the reactive potential on the basis of the solvent dependence (see below) and quantum chemical calulations.[17,18] The position at which the maximum rate of decay back to the ground state (e.g., at a conical intersection, CI) is also substituent dependent.

strong wavelength dependence in the fluorescence. The "dark" state thus populated contributes to the fluorescence through back coupling to the bright state. It is principally identified through its longer lived red-shifted transient absorption and decays to both the ground and product states. The lifetime of this dark state and its contributions to the long-lived fluorescence component are strongly dependent on the nature of the substituent. Essentially for substituents of increasing electron-withdrawing character the lifetime becomes longer and the contribution to the fluorescence smaller. We ascribe this behavior to two factors: the depth of the potential well of the dark state relative to the bright state (Figure 8a), and the coordinate(s) at which coupling of this state to the ground-state surface become large (Figure 8b).

A deeper potential well for the electron-withdrawing substituents (Figure 8a) yields the observed weaker contribution of the long component to the emission, as there is a lower probability of repopulating the bright state. Thus, the minimum energy for 1a-OMe is taken to be just below the corresponding bright state, while for 1a-CN the energy well is deeper. The apparently small difference between the structures of the Franck–Condon and relaxed state for 1a-OMe correlates with the absence of coherent motion in the ca. 100 cm^{-1} mode found in all other derivatives (Figure 4). We further propose that the minimum on the 1a-OMe excited-state surface is less displaced from the Franck–Condon state and couples strongly with the initial (1a-OMe) ground state. These factors result in a significant contribution of the 1a-OMe "dark" state to the emission and also to both its relatively fast decay (Table 2) and to the low quantum yield for formation of 1b-OMe (Table 1). In contrast the deeper well and greater displacement allows the 1a-CN dark state to be coupled to both the 1a-CN and 1b-CN ground states. This deeper trap yields the observed longer lifetime and weaker repopulation of the bright state. It also allows the dark state to decay to both the initial and the unstable (1b-CN) electronic ground states. These effects give rise to the observed longer lifetime and larger yield of 1b-CN for this derivative (Table 1). This illustrates a significant feature with regard to using substituent modulation to control motor efficiency. The highest yield for 1a-CN corresponds to the fastest fluorescence decay and the longest lived intermediate dark state. This latter feature, which we ascribe to a relatively deep potential well, allows time for the molecule to access the conical intersection and thus convert to 1b-CN. The depth of the well can evidently be controlled by the electronic character of the substituent. However, fine control also requires manipulation of the location of the conical intersection, which will certainly require quantum chemical calculation.

To compare the dynamics predicted by this model to the experimental observations, a kinetic scheme (Figure 9a) is introduced,

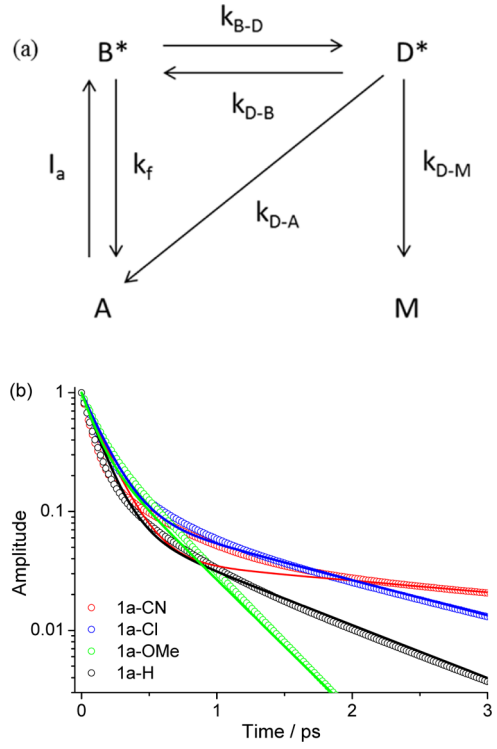

Figure 9. (a) Reduced kinetic scheme where all processes in (a) are assumed to be represented by first order kinetic. (b) Fit to the population decay data (Table 2) with the best fit kinetic parameters (Table S5).

which represents all of the relevant steps as first-order rate processes (in Figure 9a, B and D represent bright, Franck–Condon, and dark states, respectively). In this scheme the radiative transition rate k_f can be calculated from the Strickler–Berg expression (and is in the nanosecond regime), k_{BD} can be recovered from the inverse of the fastest fluorescence decay time; k_{DA} is obtained from the observed rate of ground-state recovery (assuming that process to dominate over k_f); k_{DM} is calculated from k_{DA} and the relative

dx.doi.org/10.1021/ja5041368 | J. Am. Chem. Soc. 2014, 136, 9692–9700

quantum yield, $\phi_{1a\text{-}R}/\phi_{1b\text{-}R}$ (Table 1, Supporting Information). Using these data the kinetic scheme was solved by standard matrix methods (Supporting Information) and compared with the experimental data. In this analysis k_{DB} is the only fitting parameter and is varied to achieve the best fit to the excited-state population (B), which is recovered from the integrated time-resolved emission spectra (Figure 6b).

Since the kinetic scheme does not include vibrational coherences only the exponential decay components were included in the fit. The result is shown in Figure 9b where the agreement is generally good. The only marked disagreement is for 1a-CN in the 0.5−1.5 ps region, where the measured decay was found to be non-single exponential, a feature not included in the kinetic analysis. The rate constants are collected in Table S5. The fit recovers a decreasing k_{DB} as the electron-withdrawing character of the substituent increases, consistent with the proposal of a deeper well in the dark state (Figure 8a). Thus, the PES sketched in Figure 8 provides a rationalization of the substituent-dependent time-resolved fluorescence and transient absorption data. In principle these assignments can be compared with the predictions of quantum chemical calculations. Such calculations have already begun to appear for molecules related to 1a-H. For example Filatov and co-workers reported excited-state structural dynamics as a function of twist and pyramidalization coordinates, and identified decays on two time scales and multiple conical intersections between S_1 and S_0.[17,18] Similarly Morokuma and co-workers proposed a three state relaxation mechanism also involving both double bond torsion and pyramidalization coordinates.[25] The latter calculation raises the possibility that the dark state involves an S_1/S_2 curve crossing; if that is the case the coherences observed here evidently survive the crossing. These types of calculations could usefully be extended to model the substituent effects reported here.

Probing the Reaction Coordinate. From an experimental point-of-view the nature of the reaction coordinate can be probed by studying the effects of solvent polarity and friction (viscosity) on the dynamics.[26−29] Broadly speaking large scale ultrafast structure change is expected to be resisted in viscous solvents, while a substantial increase in charge-transfer character between bright and dark states may elicit significant solvent polarity effects.

Qualitatively the 1a-R show similar solvent-dependent kinetic features in all solvents studied. The fluorescence data measured in six solvents at the wavelength of maximum intensity were all fit with (eq 1); the complete data set is presented in Table S6 along with an example of solvent-dependent fluorescence decay data (Figure S5). The coherent vibrational dynamics returned the same three frequencies in all solvents. To fit the population decay of 1a-CN three exponential decay terms were required in all solvents, two fast and one slower. For 1a-H and 1a-Cl two or three exponential decay terms were required depending on the solvent. In each case, where three components were required two of them described the fastest decay, so for the purposes of comparison among different solvents and different 1a-R, the weighted average of these two decay times is also presented. For 1a-OMe two components were adequate in all cases. The solvents varied in polarity between acetonitrile (ε_r = 37) and cyclohexane (ε_r = 2) and in viscosity from acetonitrile (η = 0.37 m Pa s^{-1}) to decalin (η = 2.5 m Pa s^{-1}) and octanol (η = 7.3 m Pa s^{-1}). In each case the fast decay time was independent of solvent within experimental error. Thus, fast relaxation out of the Franck−Condon state is determined by the shape of the potential energy surface, not the solvent, and is evidently not significantly opposed by solvent friction. This latter point is consistent with the primary dynamics involving motion along a volume conserving (thus friction insensitive) pyramidalization coordinate, rather than a significant angular torsion of the rotor/stator about the ethylenic "axle".

The slowest component in the fluorescence decay was already shown to be a strong function of substituent, being longer for electron-donating substituents (Table 2). This component is also observed to be a function of solvent viscosity. For R = H, Cl, OMe, the longest fluorescence decay time increases a factor of roughly 2.5 times between acetonitrile and octanol/decalin. This dependence suggests that motion along the coordinate responsible for this decay is resisted by solvent friction; R = CN is the exception to this trend with its weak long-lived fluorescence increasing by less than a factor of 2 in the same solvents. Significantly the slow fluorescence component is insensitive to solvent polarity in all 1a-R. The latter result suggests that evolution in the charge-transfer character of the excited states is not a key driving force in the reaction dynamics, even though the donor/acceptor character of the substituents has been modified significantly, which leads to a change in the shape of the potential energy surfaces (Figure 8).

From the preceding discussion it is anticipated that the observed viscosity dependence of the long fluorescence lifetime will be mirrored in the decay of the transient absorption and the ground-state recovery time. This is indeed the case (Figure 10, and

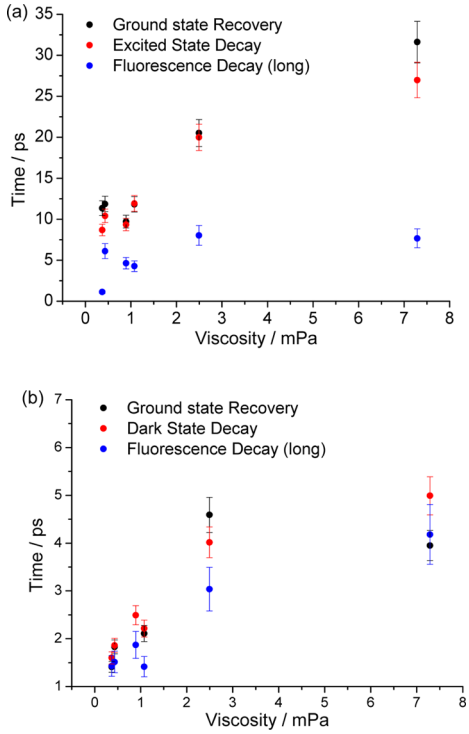

Figure 10. Comparison of the decay times for transient absorption, ground-state recovery, and time-resolved fluorescence as a function of solvent viscosity. (a) 1a-CN and (b) 1a-Cl.

Supporting Information). Both ground-state recovery and excited-state transient decay times increase monotonically with increasing viscosity but again with no marked polarity effect. This confirms that the coordinate responsible for decay from the dark state to the ground state is friction dependent, and thus probably involves a large scale intramolecular motion, most likely (and in agreement

dx.doi.org/10.1021/ja5041368 | J. Am. Chem. Soc. 2014, 136, 9692−9700

with calculations[17,18]) some degree of torsion about the ethylenic "axle". This viscosity dependence is also seen for the long lifetime of the 1a-CN dark state but is not reflected in the time-resolved fluorescence (Figure 10). Again it is unclear whether this reflects limitations due the low signal-to-noise ratio associated with the very weak slow fluorescence of this derivative or a genuinely more complex relaxation from its dark state.

CONCLUSION

The excited-state dynamics of a family of chiral overcrowded alkene-based photoactivated molecular motors, 1a-R, were studied as a function of the electron donor/acceptor character of the substituent conjugated with the central "axle" double bond. The nature of the substituent was shown to have a significant effect on the excited-state potential energy surfaces, modifying the excited-state dynamics and leading to a substituent-dependent quantum yield of isomerization. This behavior is in contrast to the thermal reaction in the electronic ground state, which is insensitive to substituent.[10] The primary event in the excited state is ultrafast relaxation out of the Franck−Condon excited state on a 100 fs time scale. This primary step populates a dark excited state, which remains coupled to the Franck−Condon state but decays on a picosecond time scale to the ground state. The effect of the substituent on the dynamics was traced to its modulation of the energy and position of the minimum of the dark-state potential. These parameters can be tuned by the electronic character of the substituent, thus modifying the efficiency of the motors.

The nature of the coordinates involved in the relaxation was probed through the effect of solvent. The dynamics are essentially independent of solvent polarity, suggesting intramolecular charge transfer and subsequent solvation dynamics is not the major driving force. The primary 100 fs relaxation was also insensitive to solvent viscosity and thus involves a volume conserving structure change, possibly pyramidalization at C9 of the ethylenic "axle" bond. The picosecond relaxation of the dark state is sensitive to solvent viscosity, consistent with an assignment to torsional motion about the double bond. These coordinates and the effect of substituents on them could be further probed through quantum chemical calculations.

EXPERIMENTAL SECTION

The series 1a-R were synthesized and purified as previously described.[14] Solutions for ultrafast measurements had a concentration <1 mM. Time-resolved fluorescence was measured with 50 fs time resolution using the up-conversion method described in detail elsewhere.[30] The transient absorption experiment had lower (ca. 300 fs) time resolution and has also been outlined previously.[31] The data analysis protocols for transient data were described earlier.[11] In all kinetics experiments the excitation wavelength used was 400 nm. Steady-state fluorescence spectra were recorded at lower concentrations (tens of μM) with excitation at 370 nm and Raman and solvent contributions were subtracted.

ASSOCIATED CONTENT

Supporting Information

Additional experimental details, detailed numerical tables from fitting the transient data and additional transient data. This material is available free of charge via the Internet at http://pubs.acs.org.

AUTHOR INFORMATION

Corresponding Author

s.meech@uea.ac.uk

Notes

The authors declare no competing financial interest.

ACKNOWLEDGMENTS

We are grateful for financial support from EPSRC (EP/E010466, to S.R.M), and the ERC (Starting Grant 279549, to W.R.B., and Advanced Investigator Grant 227897, to A.C., B.L.F.). J.C. was supported by a University of East Anglia studentship. We are grateful to Dr. Garth Jones (UEA) for assistance with the TD-DFT calculation.

REFERENCES

(1) Kinbara, K.; Aida, T. *Chem. Rev.* **2005**, *105*, 1377.
(2) Peterman, E. J. G.; Sosa, H.; Moerner, W. E. *Annu. Rev. Phys. Chem.* **2004**, *55*, 79.
(3) Schliwa, M.; Woehlke, G. *Nature* **2003**, *422*, 759.
(4) Vale, R. D. *Cell* **2003**, *112*, 467.
(5) Feringa, B. L. *Acc. Chem. Res.* **2001**, *34*, 504.
(6) Koumura, N.; Zijlstra, R. W. J.; van Delden, R. A.; Harada, N.; Feringa, B. L. *Nature* **1999**, *401*, 152.
(7) Koumura, N.; Geertsema, E. M.; van Gelder, M. B.; Meetsma, A.; Feringa, B. L. *J. Am. Chem. Soc.* **2002**, *124*, 5037.
(8) Vicario, J.; Meetsma, A.; Feringa, B. L. *Chem. Commun.* **2005**, 5910.
(9) Klok, M.; Boyle, N.; Pryce, M. T.; Meetsma, A.; Browne, W. R.; Feringa, B. L. *J. Am. Chem. Soc.* **2008**, *130*, 10484.
(10) Klok, M.; Janssen, L.; Browne, W. R.; Feringa, B. L. *Faraday Discuss.* **2009**, *143*, 319.
(11) Conyard, J.; Addison, K.; Heisler, I. A.; Cnossen, A.; Browne, W. R.; Feringa, B. L.; Meech, S. R. *Nat. Chem.* **2012**, *4*, 547.
(12) Perez-Hernandez, G.; Pelzer, A.; Gonzalez, L.; Seideman, T. *New J. Phys.* **2010**, *12*, 24.
(13) Yamaki, M.; Hoki, K.; Kono, H.; Fujimura, Y. *Chem. Phys.* **2008**, *347*, 272.
(14) Pollard, M. M.; Meetsma, A.; Feringa, B. L. *Organic & Biomolecular Chemistry* **2008**, *6*, 507.
(15) Pollard, M. M.; Wesenhagen, P. V.; Pijper, D.; Feringa, B. L. *Org. Biomol. Chem.* **2008**, *6*, 1605.
(16) Pollard, M. M.; Klok, M.; Pijper, D.; Feringa, B. L. *Adv. Funct. Mater.* **2007**, *17*, 718.
(17) Kazaryan, A.; Kistemaker, J. C. M.; Schafer, L. V.; Browne, W. R.; Feringa, B. L.; Filatov, M. *J. Phys. Chem. A* **2010**, *114*, 5058.
(18) Kazaryan, A.; Lan, Z.; Schafer, L. V.; Thiel, W.; Filatov, M. *J. Chem. Theory Comput.* **2011**, *7*, 2189.
(19) Takeuchi, S.; Ruhman, S.; Tsuneda, T.; Chiba, M.; Taketsugu, T.; Tahara, T. *Science* **2008**, *322*, 1073.
(20) Mokhtari, A.; Chebira, A.; Chesnoy, J. *J. Opt. Soc. Am. B* **1990**, *7*, 1551.
(21) Bardeen, C. J.; Wang, Q.; Shank, C. V. *Phys. Rev. Lett.* **1995**, *75*, 3410.
(22) Vos, M. H.; Rappaport, F.; Lambry, J. C.; Breton, J.; Martin, J. L. *Nature* **1993**, *363*, 320.
(23) McClure, S. D.; Turner, D. B.; Arpin, P. C.; Mirkovic, T.; Scholes, G. D. *J. Phys. Chem. B* **2014**, *118*, 1296.
(24) Rubtsov, I. V.; Yoshihara, K. *J. Phys. Chem. A* **1999**, *103*, 10202.
(25) Liu, F.; Morokuma, K. *J. Am. Chem. Soc.* **2012**, *134*, 4864.
(26) Kim, H. J.; Hynes, J. T. *Int. J. Quantum Chem.* **1990**, 821.
(27) Fleming, G. R.; Cho, M. H. *Annu. Rev. Phys. Chem.* **1996**, *47*, 109.
(28) Hynes, J. T. *Annu. Rev. Phys. Chem.* **1985**, *36*, 573.
(29) van der Zwan, G.; Hynes, J. T. *J. Chem. Phys.* **1983**, *78*, 4174.
(30) Heisler, I. A.; Kondo, M.; Meech, S. R. *J. Phys. Chem. B* **2009**, *113*, 1623.
(31) Lukacs, A.; Zhao, R. K.; Haigney, A.; Brust, R.; Greetham, G. M.; Towrie, M.; Tonge, P. J.; Meech, S. R. *J. Phys. Chem. B* **2012**, *116*, 5810.